Volume 12 Number 2
Journal of Advances in Physics

Characterization of Indium addition on Sn-Bi-Sb Lead free Solder alloy

S. Mosaad [(1,*)], A. R. Mohamed[2], Mustafa Kamal[3]
[(1,*)] Physics Department, Faculty of Science, Suez Canal University, Egypt
saramosaad@windowslive.com
[2] Physics Department, Faculty of Science, Port Said University, Egypt
raoufahmed@yahoo.com
[3] Metal Physics lab. Physics Department, Faculty of Science, Mansoura University, Egypt
kamal42200274@yahoo.com

Abstract

The aim of these work is to measure the effect of the addition of In with different atomic percent weight on structure, melting, Electrical and mechanical properties of Sn_{70-X} at.% -Bi_{15} at.% -Sb_{15} at.%- In_x at.% rapidly solidified. X-ray diffraction analysis (XRD), differential scanning calorimetry (DSC), temperature dependence of resistivity (TDR), and mechanical resonance method are performed. It's found that electrical conductivity (σ) and thermal conductivity (K) increased gradually by increasing In at.%. Melting temperature reduced from 470.12 K for Sn_{70} at.%- Bi_{15} at.%- Sb_{15} at.% to 427.13 K in Sn_{61} at.%- Bi_{15} at.%- Sb_{15} at.%- In_9 at.%. Also, elastic moduli, internal friction and thermal diffusivity measured from melt-quenched ribbons.

Keywords

Rapid Solidification (RS); Lead Free Solder Alloys; Sn-Bi-Sb, X-Ray Diffraction Analysis (XRD); Electrical Resistivity; Thermal analysis ; Mechanical properties.

Academic Discipline And Sub-Disciplines

Physics; Solid State Physics

SUBJECT CLASSIFICATION

Solder alloy

TYPE (METHOD/APPROACH)

Experimental

Introduction

In recent years, substantial efforts were made to develop lead-free solders that are suitable substitutes for classic tin-lead eutectic solders [1]. There is a growing need for solders that can be used for applications with more demanding service conditions such as in Sealing in cryogenic applications, Soldering or fusing applications High-end device cooling by reduces operating temperatures. For these purposes, it is necessary to evaluate the properties of candidate solder alloys that are related to manufacturing and reliability. There are many different metals and metal alloys that can be used as solders and a set of binary alloys have been chosen as candidates for lead-free solders those are: Sn-Bi, Sn-Sb, Sn-Cu, and Sn-Zn. Among the ternary compositions, the Sn-Bi-Zn is used in making printing wiring boards [2]. However all of these eutectic compositions have a melting temperature above 473 K. Among the commercial Lead-free alloys, Sn-58 wt% Bi eutectic alloy may be a favorable alloy especially for electronics and telecommunications. In fact, this alloy, which has the eutectic temperature of 412 K and has a higher ultimate tensile stress and shear strength over Sn-Pb eutectic [3,4]. Bismuth has also been used as the alloying element in ternary Sn-Zn-Bi Sn-Ag-Bi and Sn-Bi-Cu systems to provide suitable substitutes for Sn-Pb solder alloys [5, 6, 7, and 8].

Indium also chosen in solder alloys because of Indium is ductile and malleable that makes it to deform and fill in the uneven microstructure of two mating parts, by only moderate pressure. This ductility and malleability is retained at cryogenic temperatures so that an assembly can maintain the effective seal, even in harsh environments. At relatively high thermal conductivity of 86W/mK at 85°C, indium is widely used in the applications of thermal management to dissipate the heat produced by electronic components. Indium compensates for different coefficients of thermal expansion (CTE) during bonding dissimilar parts. At small percentages, indium can improve the thermal fatigue performance of solders that used in electronics assembly. Indium alloys enable solders to withstand drop tests better than other low melting alloy. Several indium-containing alloys that melt at temperatures less than 180°C, could be used as step soldering or applications that require lower reflow temperatures. Indium has a low vapor pressure, making it suitable for use in high vacuum applications.

The effect of Sn on reversibility of liquid –liquid transition in Bi-Sb-Sn alloys had been done by Xianfen Li et al and the results show that Sn plays an important role on the reversibility of liquid-liquid transition [8]. Dragan Manasijevic et al have studied experimentally the phase equilibria and thermodynamics of the Bi-Sb-Sn ternary system [9]. Y.S. Hor and R.J. Cava have reported the thermoelectric properties of Sn-doped Bi-Sb that small amounts of Sn doping dramatically decrease the thermal conductivity of the alloy system using melt stoichiometric mixtures of elemental Bi,Sb and Sn in 4mm inner diameter quartz tube [10]. Alberto Torres et al had performed and studied the effects of adding of Sb (0, 3 and 6wt. %) of Sn-Bi eutectic solder alloys on structure, melting, corrosion and mechanical properties [11]. Thermodynamic

database for phase diagram in Sn-Sb-Bi ternary alloy system have been investigated by Ohnuma et al and thermodynamic calculation on the Sn-Sb-Bi showed by [12-18].

The aim of this study was to investigate the effects of In content on structure, electrical, thermal and mechanical properties of all melt-quenched ribbons of Sn_{70-x}-Bi_{15}-Sb_{15}-In_x (where x= 0, 1, 3, 5, 7, and 9 in at. %) that promote the application of SnBiSbIn series alloys on the functionality industry.

Experimental procedures

The materials used in the present work are Sn, Sb, Bi, and In fragments, with purity was better than 99.99% produced by a single copper roller (200 mm in diameter) melt-spinning technique [19-23]. The process parameters such as the ejection temperature, and the linear speed of the wheel were fixed at 873 K and 30.4 ms^{-1} respectively. X-ray diffraction analysis (XRD) was carried out with a XPERT-PRO X-ray diffractometer, using Cu-Kα radiation of λ = 1.5406 Å. Differential Scanning Calorimetry (DSC) was carried out in a Shimadzu (DSC-50) with heating rate at 10 $K{\cdot}min^{-1}$. The temperature dependence of resistivity (TDR) was measured by four probe method using micro ohmmeter of type BS407. The BS407 uses a four terminal measurement system via high quality Kelvin Clip leads with sensitivity is 1 μΩ. The heating range starts from room temperature up to 480 K with heating rate of 5 $K{\cdot}min^{-1}$. Elastic moduli, the internal friction and the thermal diffusivity of melt-spun ribbons were examined in air atmosphere with a modified dynamic resonance method [24].

2- Results and Discussion

2.1 Structure

Figure (1) shows the X-ray diffraction pattern for as-quenched melt-spun of Sn_{70-x}-Bi_{15}-Sb_{15}-In_x alloys (where x= 0, 1, 3, 5, 7, and 9 in at. %). The experimentally results show interplanar spacing's of the first few strong reflections are tabulated in Table (1). The pattern can be indexed in terms of the co-existence of Tetragonal Sn, Rhombohedral Sb and Bi phases, Tetragonal In, and intermediate compounds. Such as Rhombohedral SnSb and Orthorhombic InSn, Tetragonal Bi_3In_5, Hexagonal $In_{0.2}Sn_{0.8}$.

The XRD for Sn_{70}-Bi_{15}-Sb_{15} alloy is shown in Figure 1(a), Sn, Bi and Sb are precipitated as indicated and SnSb Intermetallic compound is appeared. The unit cell of β-Sn is body centered tetragonal (S.G.: I41/amd).

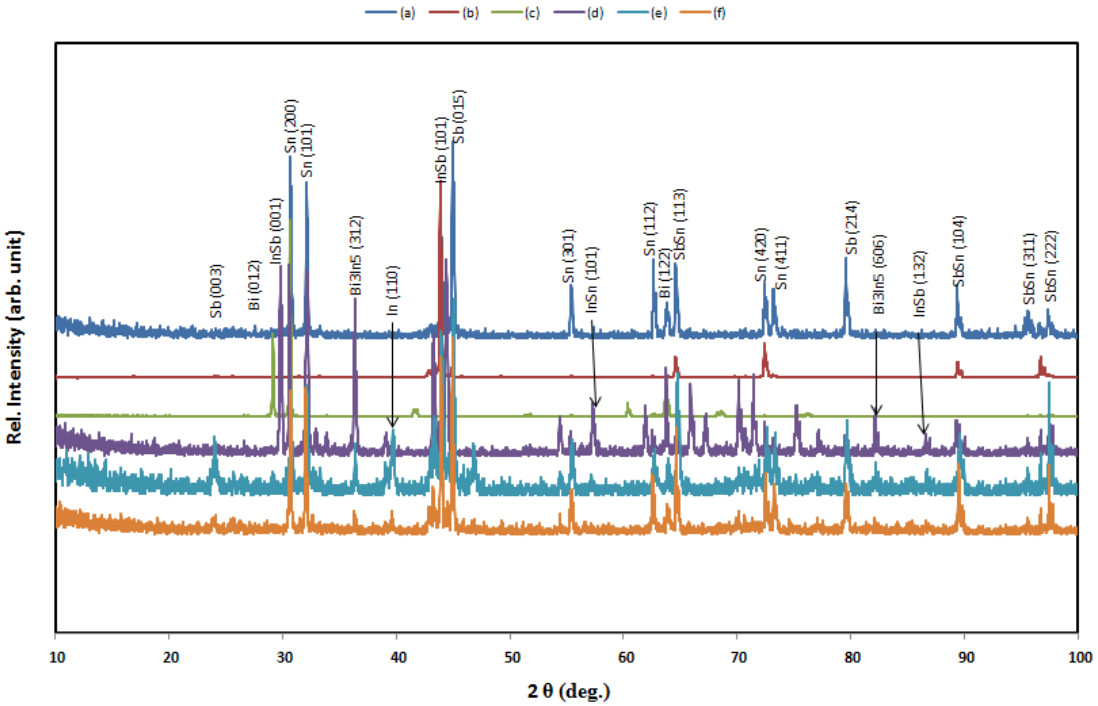

Figure 1. The XRD patterns for as-quenched melt-spun alloys. (a) Sn_{70}-Bi_{15}-Sb_{15}; (b) Sn_{69}-Bi_{15}-Sb_{15}-In_1; (c) Sn_{67}-Bi_{15}-Sb_{15}-In_3; (d) Sn_{65}-Bi_{15}-Sb_{15}-In_5; (e) Sn_{63}-Bi_{15}-Sb_{15}-In_7 and (f) Sn_{61}-Bi_{15}-Sb_{15}-In_9 in at %.

The crystal structure of Bi is Rhombohedral-hexagonal (S.G.: R3m). The unit cell of Sb is Rhombohedral (S.G.: R-3m). The unit cell of SbSn is Rhombohedral (S.G.: R-3m).

Figure 1(b) shows for Sn_{69}-Bi_{15}-Sb_{15}-In_1 alloy, it is clear that Sb phase and SnSb Intermetallic compound are disappeared and there is an existence of new Intermetallic compound, these are, InSb with Orthorhombic crystal structure (S.G.: Pmmn), and Bi_3In_5 Intermetallic phase with Tetragonal unit cell (S.G.: 14/mcm). It is notice that Sn phase and Bi phase exist in these positions.

Figure 1(c) for Sn_{67}-Bi_{15}-Sb_{15}-In_3 alloy show that SnSb Intermetallic compound comeback with the absence of Sb phase and existence of InSb and Bi_3In_5. By Increasing In at.% as in Sn_{65}-Bi_{15}-Sb_{15}-In_5 alloy (Figure 1(d)) will show that a new phases are formed these are In Intermetallic phase with Tetragonal unit cell (S.G.: 14/mmm) and $In_{0.2}Sn_{0.8}$ with Hexagonal crystal structure (S.G.: P6/mmm). SnSb Intermetallic phase returns to appear again in the absence of Sb phase.

Figure 1(e) show Sn_{63}-Bi_{15}-Sb_{15}-In_7 alloy and figure 1(f) show Sn_{61}-Bi_{15}-Sb_{15}-In_9 alloy, It quite clear that, in these two alloys, the all intermediate phases are exist and which may be evidence that In atomic percent become enough for the exists of all phases. XRD analysis is shown in Table 1.

Figure 2(a) shows the variation of the axial ratio c/a with In concentration and figure 2(b) shows the variation of the volume of unit cell of Sn phase with In concentrations. It is clear that, there is a drop at axial ratio at Sn_{65}-Bi_{15}-Sb_{15}-In_5 alloy without these point all values of axial ratio increased by increasing In concentration. From the figure 2 (b), it is clear that the volume of unit cell of Sn has a variation and the highest value belongs to Sn_{67}-Bi_{15}-Sb_{15}-In_3 alloy and the lowest value belongs to Sn_{63}-Bi_{15}-Sb_{15}-In_7.

In general each unit cell contains an integer number of atoms and the crystal structure is attributed to a crystallographic system for a crystal tin. In practice, a cell containing a non-integer number of atoms as indicated in Table (II), it is well known that cell, usually contains point defects. The distribution of point defects could have a short range order and it varies from cell to cell.

The uniform macro strain causes a shift of the direction lines to

new 2Θ positions . This non-uniform micro strain causes a broadening of the corresponding diffraction line [25]. Line width B, both full width at half maximum (FWHM) and integral breadth, were used a Williamson-Hall plot [26] as illustrated in figure (3).

Table 1. The XRD patterns details for as-quenched melt-spun alloys. Sn_{70}-Bi_{15}-Sb_{15}; Sn_{69}-Bi_{15}-Sb_{15}-In_1; Sn_{67}-Bi_{15}-Sb_{15}-In_3; Sn_{65}-Bi_{15}-Sb_{15}-In_5; Sn_{63}-Bi_{15}-Sb_{15}-In_7 and Sn_{61}-Bi_{15}-Sb_{15}-In_9 in at %.

Alloy	Phase present	hkl	The lattice parameter for each phase				Crystal structure
			a (Å)	c (Å)	v (Å^3)	c/a	
Sn_{70}-Bi_{15}-Sb_{15}	Sn	200	5.8177	3.1697	107.2854	0.5448	Tetragonal (S.G.: I41/amd)
	Bi	012	4.6166	11.8450	218.6304	2.5657	Rho.-hex. (S.G.: R3m)
	Sb	003	4.4346	11.2270	191.2017	2.5316	Rho. (S.G.: R-3m)
	SbSn	021	4.2007	4.5947	70.2147	1.0937	Rho. (S.G.: R-3m)
Sn_{69}-Bi_{15}-Sb_{15}-In_1	Sn	200	5.8231	3.1754	107.6763	0.5453	Tetragonal (S.G.: I41/amd)
	Bi	012	4.6821	11.8876	225.6854	2.5389	Rho.-hex. (S.G.: R3m)
	InSb	201	5.6627	3.15854	91.6919	0.5577	Ortho. (S.G.: Pmmn)
	Bi_3In_5	312	8.6347	12.5978	939.2919	1.4589	Tetragonal (S.G.: 14/mcm)
Sn_{67}-Bi_{15}-Sb_{15}-In_3	Sn	200	5.8281	3.1781	107.9526	0.5453	Tetragonal (S.G.: I41/amd)
	Bi	012	4.5599	11.8376	213.1557	2.5960	Rho.-hex. (S.G.: R3m)
	SbSn	021	4.2007	4.5947	70.2147	1.0937	Rho. (S.G.: R-3m)
	InSb	201	5.8588	3.0461	95.0713	0.5199	Ortho. (S.G.: Pmmn)
	Bi_3In_5	312	8.4549	12.2575	876.2421	1.4497	Tetragonal (S.G.: 14/mcm)
Sn_{65}-Bi_{15}-Sb_{15}-In_5	Sn	200	5.8369	3.1618	107.7234	0.5416	Tetragonal (S.G.: I41/amd)
	Bi	012	4.5368	11.9134	245.210	2.6259	Rho.-hex. (S.G.: R3m)
	In	110	3.2592	4.9436	52.5148	1.5168	Tetragonal (S.G.: 14/mmm)
	SbSn	021	4.2995	5.4140	100.0822	1.2592	Rho. (S.G.: R-3m)
	InSb	201	5.7350	3.04769	93.2001	0.5314	Ortho. (S.G.: Pmmn)
	Bi_3In_5	312	8.5908	12.7456	940.658	1.4836	Tetragonal (S.G.: 14/mcm)
	$In_{0.2}Sn_{0.8}$	001	3.2188	2.99397	31.02095	0.9301	Hexagonal (S.G.: P6/mmm)

Sn_{63}-Bi_{15}-Sb_{15}-In_7	Sn	200	5.8098	3.1732	107.1093	0.5461	Tetragonal (S.G.: I41/amd)
	Bi	012	4.5240	11.8774	210.5206	2.6254	Rho.-hex. (S.G.: R3m)
	Sb	003	4.2077	11.0841	169.9503	2.6342	Rho. (S.G.: R-3m)
	In	110	3.2807	4.95398	53.32261	1.5099	Tetragonal (S.G.: 14/mmm)
	SbSn	021	4.3105	5.4191	87.2002	1.2571	Rho. (S.G.: R-3m)
	InSb	201	5.8104	2.9958	93.5626	0.5155	Ortho. (S.G.: Pmmn)
	Bi_3In_5	312	8.4761	12.5979	905.0973	1.4862	Tetragonal (S.G.: 14/mcm)
	$In_{0.2}Sn_{0.8}$	001	3.2188	2.9782	26.7219	0.9252	Hexagonal (S.G.: P6/mmm)
Sn_{61}-Bi_{15}-Sb_{15}-In_9	Sn	200	5.8217	3.1795	107.7626	0.5461	Tetragonal (S.G.: I41/amd)
	Bi	012	4.5541	11.6544	209.3273	2.5590	Rho.-hex. (S.G.: R3m)
	Sb	003	4.2249	11.1293	172.0416	2.6341	Rho. (S.G.: R-3m)
	In	110	3.2200	4.94608	51.2843	1.5360	Tetragonal (S.G.: 14/mmm)
	SbSn	021	4.3643	5.0089	82.6250	1.1476	Rho. (S.G.: R-3m)
	InSb	201	5.7538	3.03903	94.8620	0.5281	Ortho. (S.G.: Pmmn)
	Bi_3In_5	312	8.7284	12.5251	954.2467	1.4349	Tetragonal (S.G.: 14/mcm)
	$In_{0.2}Sn_{0.8}$	001	3.2193	3.0777	31.8993	0.9560	Hexagonal (S.G.: P6/mmm)

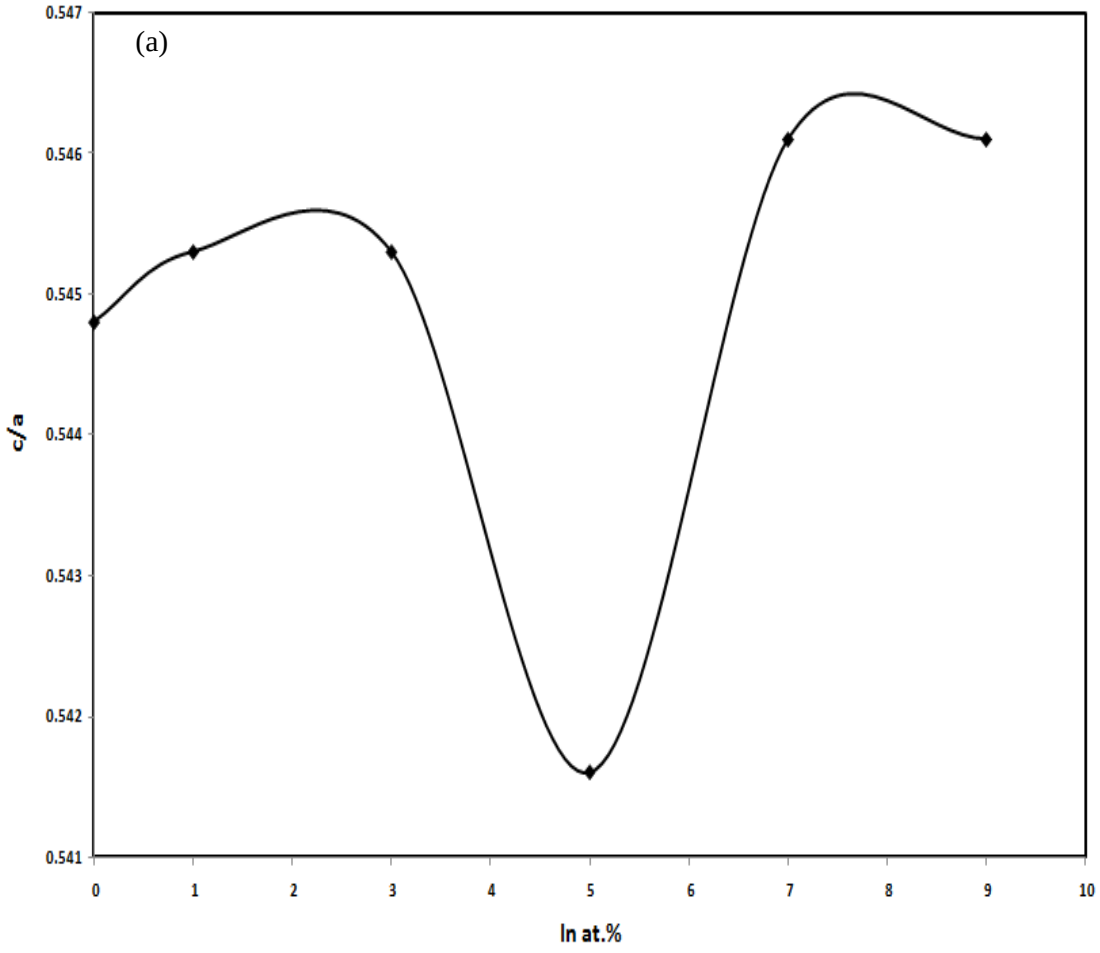

ISSN 2347-3487
Volume 12 Number 2
Journal of Advances in Physics

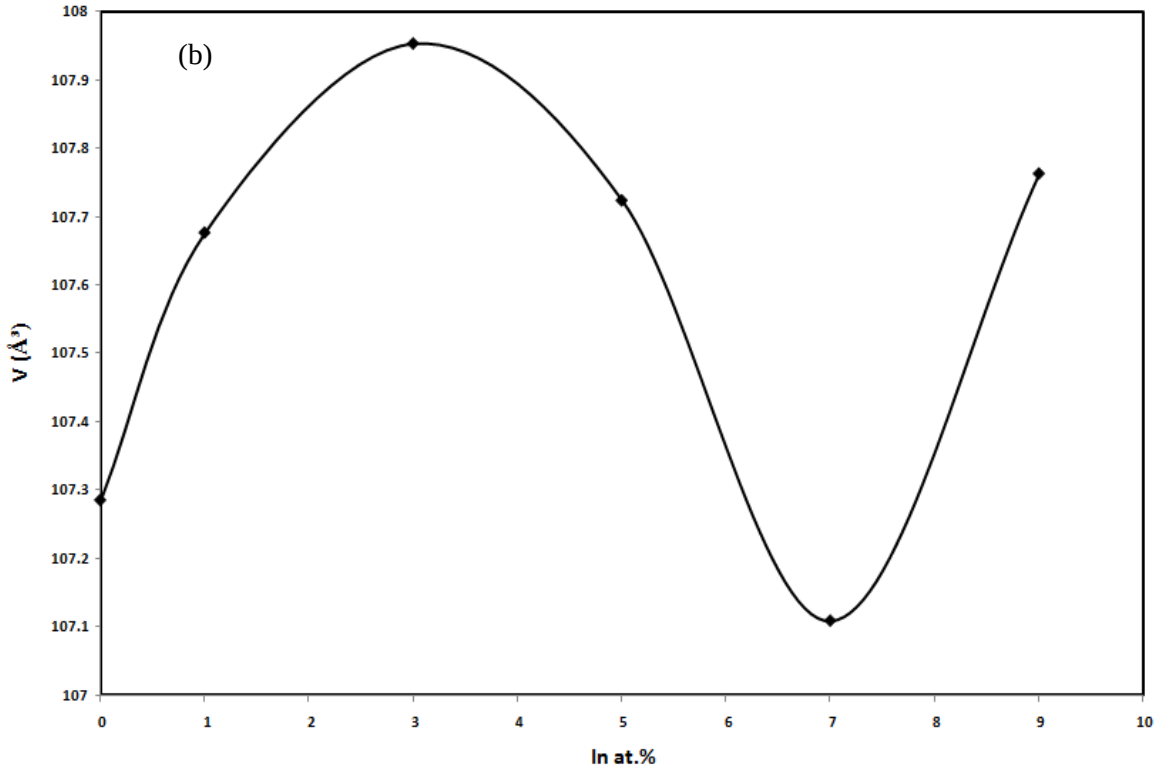

Figure 2. (a) The variation of c/a with Incc concentration; (b) The variation of v with In concentration

Table (II). Structural data of Sn phases in prepared alloys.

Alloy	ρ (g/cm^3)	n. of atoms / cell	1/D_{eff} (Å^{-1}) (10^{-3})	5<ε^2>$^{1/2}$ (10^{-3})
Sn_{70}-Bi_{15}-Sb_{15}	5.714286	3.110677	6.39	10.34
Sn_{69}-Bi_{15}-Sb_{15}-In_1	7.976974	4.358234	3.63	0.5339
Sn_{67}-Bi_{15}-Sb_{15}-In_3	6.428571	3.521277	2.97	18.7
Sn_{65}-Bi_{15}-Sb_{15}-In_5	5.928571	3.240503	6.28	13.35
Sn_{63}-Bi_{15}-Sb_{15}-In_7	5.535714	3.008522	6.36	96
Sn_{61}-Bi_{15}-Sb_{15}-In_9	4.587912	2.508623	4.82	39.7

To find information about the crystallite size D_{eff} and local lattice distortion $< \Sigma^2 >$ in tin phases, the following equation may be used:

$$\beta = \left(\frac{1}{D_{eff}}\right) + 5 < \Sigma^2 >^{1/2} \sin\theta/\lambda \qquad (1)$$

The $1/D_{eff}$ and $5 < \Sigma^2 >^{½}$ parameters are given in Table (II). For the Sn phase is immeasurably low, leads to a good crystallization state. The results are discussed predominantly in terms of the size and strain values obtained.

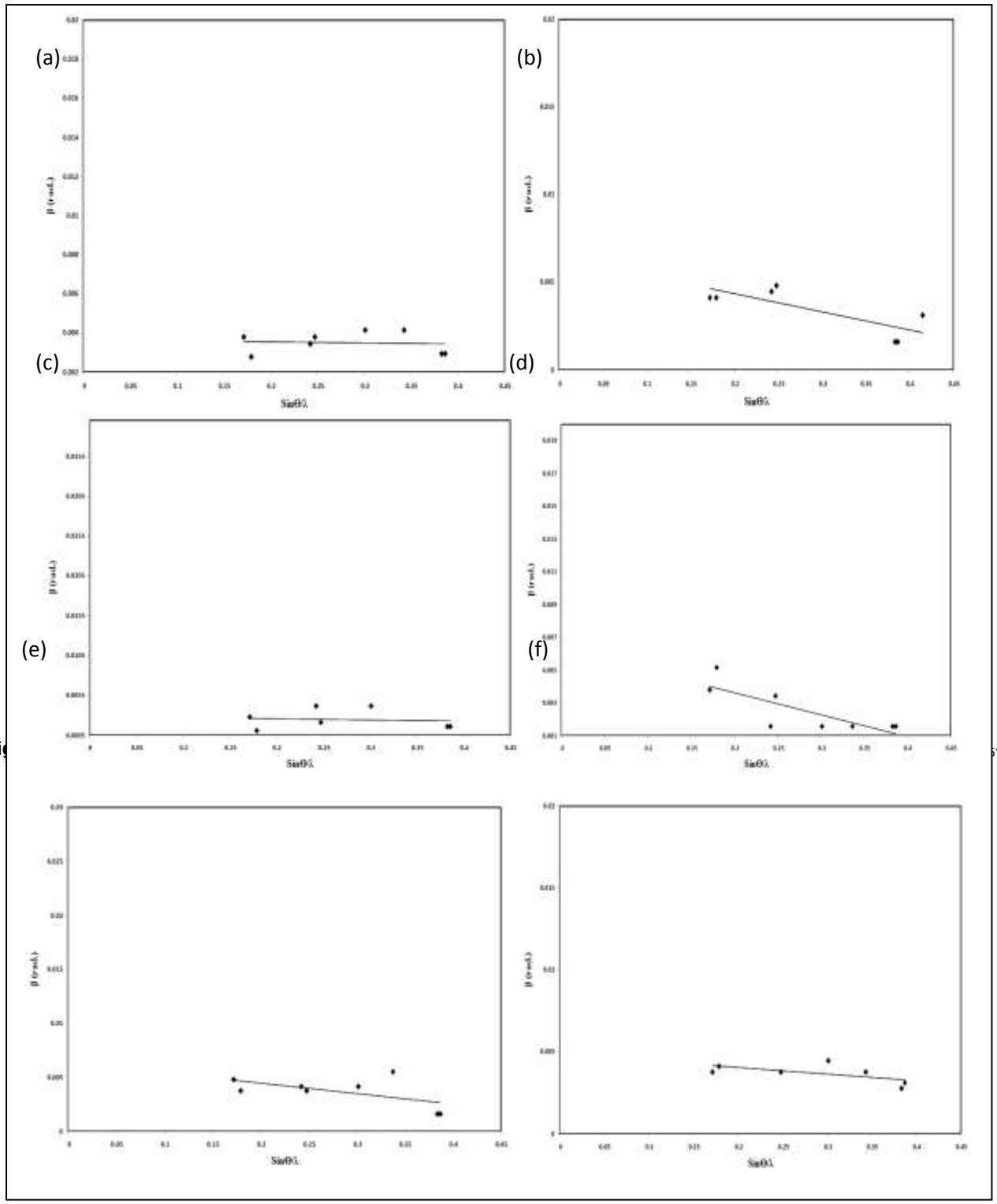

Figure 3. Crystallite size and lattice distortion of Sn phase in (a) Sn_{70}-Bi_{15}-Sb_{15}; (b) Sn_{69}-Bi_{15}-Sb_{15}-In_1; (c) Sn_{67}-Bi_{15}-Sb_{15}-In_3; (d) Sn_{65}-Bi_{15}-Sb_{15}-In_5; (e) Sn_{63}-Bi_{15}-Sb_{15}-In_7 and (f) Sn_{61}-Bi_{15}-Sb_{15}-In_9 in at % alloys.

2.2 Thermal Analysis

Figure (4) shows the DSC curves for as-quenched melt-spun pure Sn_{70-x}-Bi_{15}-Sb_{15}-In_x (x = 0, 1, 3, 5, 7 and 9 in at %) alloys. The endothermic peak due to melting was obtained, the melting temperature T_m and the enthalpy of fusion ΔH_m have been determined. ΔH_m was obtained from the integral under the DSC peak of melting as given by equation:

$$\Delta H_m = \int_{T_0}^{T_f} C_p \, dt \qquad (2)$$

Where, C_p is the heat capacity at constant pressure, T_0 and T_f are known as onset melting temperature and final melting temperature of the specimen, respectively. Table (III) shows DSC results. It is evident that the melting temperature

ISSN 2347-3487
Volume 12 Number 2
Journal of Advances in Physics

decreases by increasing In concentration from 473 K for Sn_{70}-Bi_{15}-Sb_{15} to 432.65 K for Sn_{61}-Bi_{15}-Sb_{15}-In_9 alloy. The enthalpy of fusion ΔH_m and the entropy ΔS decreases by increasing In for all alloys except for Sn_{65}-Bi_{15}-Sb_{15}-In_5 and Sn_{69}-Bi_{15}-Sb_{15}-In_1 alloys.

The pasty range is very important parameter in solder, the highest value calculated to be 15.5 for Sn_{63}-Bi_{15}-Sb_{15}-In_7 alloy and the lowest value is 7.59 for Sn_{69}-Bi_{15}-Sb_{15}-In_1 alloy.

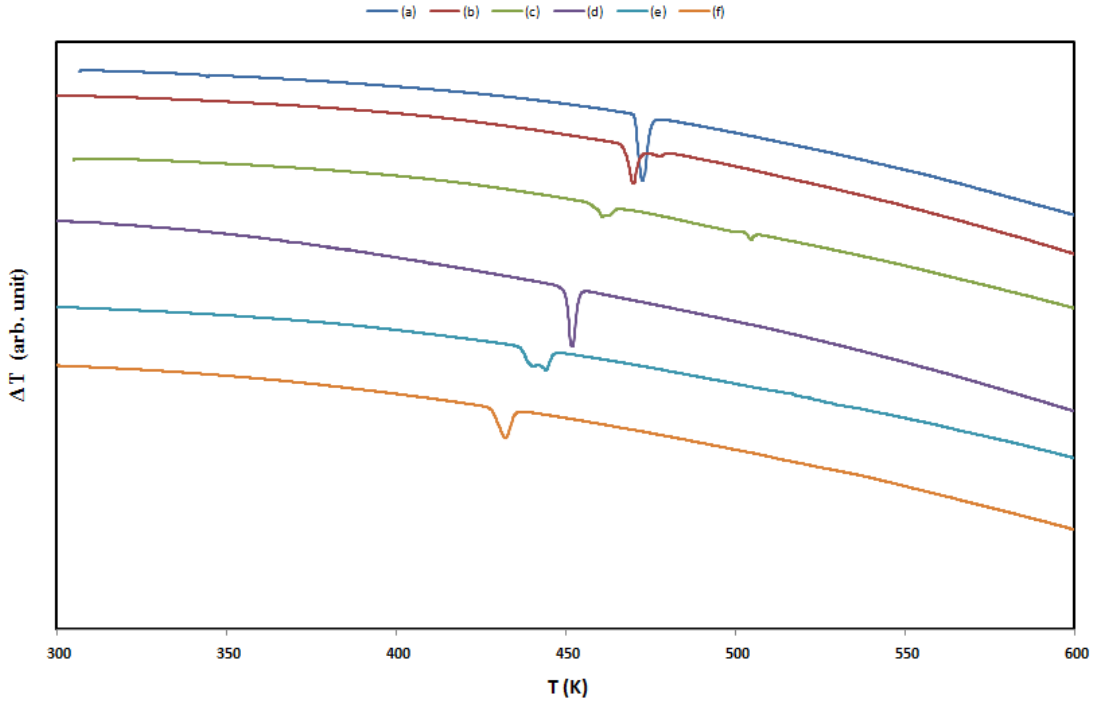

Figure 4. The DSC curves for as-quenched melt-spun alloys (a) Sn_{70}-Bi_{15}-Sb_{15}; (b) Sn_{69}-Bi_{15}-Sb_{15}-In_1; (c) Sn_{67}-Bi_{15}-Sb_{15}-In_3; (d) Sn_{65}-Bi_{15}-Sb_{15}-In_5; (e) Sn_{63}-Bi_{15}-Sb_{15}-In_7 and (f) Sn_{61}-Bi_{15}-Sb_{15}-In_9 in at % alloys.

Table (III). The DSC Details for as-quenched melt-spun alloys.

Alloy	T_0 (K)	T_f (K)	T_m (K)	Pasty range	ΔH_m (KJ/Kg)	ΔS (J/Kg.K)
Sn_{70}-Bi_{15}-Sb_{15}	470	478	473	8	56.34615	119.12505
Sn_{69}-Bi_{15}-Sb_{15}-In_1	466.03	473.62	470.24	7.59	39.25	83.468016
Sn_{67}-Bi_{15}-Sb_{15}-In_3	455.65	466.18	460.77	10.53	19.09	41.430649
Sn_{65}-Bi_{15}-Sb_{15}-In_5	444.3	456.8	451.74	12.5	59.3	131.2702
Sn_{63}-Bi_{15}-Sb_{15}-In_7	436.52	452.02	440.92	15.5	10.53	23.881883
Sn_{61}-Bi_{15}-Sb_{15}-In_9	427.13	436.92	432.65	9.79	47.21	109.11822

2.3 Electrical properties

Figure (5) shows the temperature dependence of resistivity obtained for as-quenched melt-spun Sn_{70-x}-Bi_{15}-Sb_{15}-In_x , x = 0, 1, 3, 5, 7, and 9) alloy in the temperature range from 300 to 450 K. The behavior is metallic, that mean the resistivity increases by increasing temperature. The resistivity at room temperature ρ is found to be $239.088 * 10^{-8}$ Ω.m for Sn_{70}-Bi_{15}-Sb_{15} alloy. By increasing In content, the resistivity decreases linearly up to $92.5 * 10^{-8}$ (Ω.m), which shown in Table (IV) and figure 6 (a). The temperature coefficient of resistivity TCR was calculated to be 14.05×10^{-3} K^{-1} for Sn_{70}-Bi_{15}-Sb_{15} alloy. The TCR decreased due to the addition of In as shown in figure 6 (b).

Table (V) gives a list of the electrical conductivities and other transport parameters of the studied quenched ribbons from the melt. Values of the concentrations of conduction electrons, mobility (μ) , collision time (ι) and mean free Path (*l*) are also given accordingly to the quantum theory [29] .

ISSN 2347-3487
Volume 12 Number 2
Journal of Advances in Physics

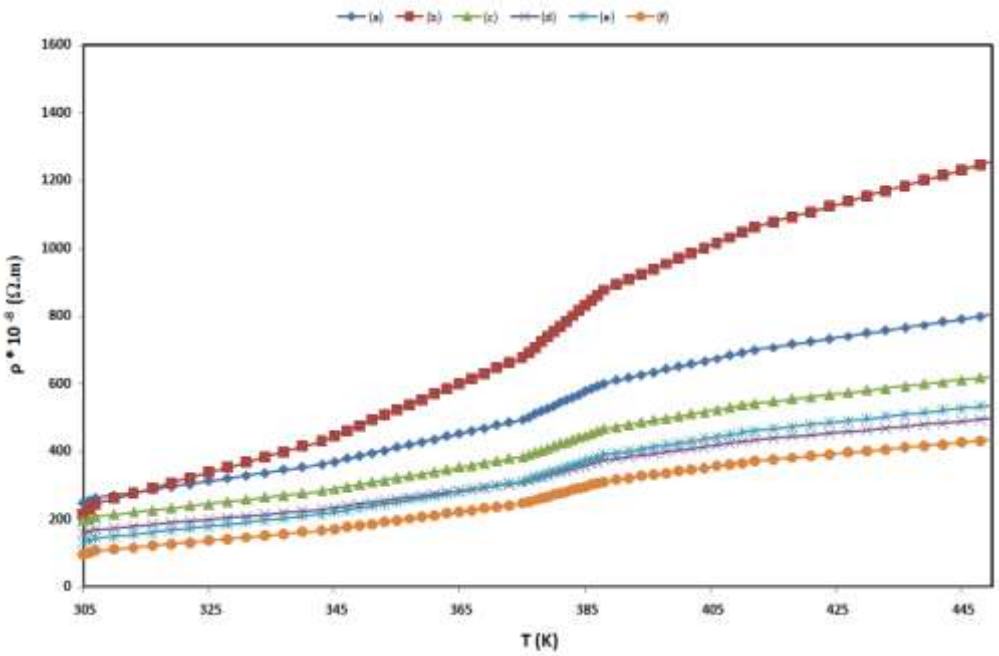

Figure 5. The TCR curves for as-quenched melt-spun alloys (a) Sn_{70}-Bi_{15}-Sb_{15}; (b) Sn_{69}-Bi_{15}-Sb_{15}-In_1; (c) Sn_{67}-Bi_{15}-Sb_{15}-In_3; (d) Sn_{65}-Bi_{15}-Sb_{15}-In_5; (e) Sn_{63}-Bi_{15}-Sb_{15}-In_7 and (f) Sn_{61}-Bi_{15}-Sb_{15}-In_9 in at % alloys.

Table (IV). Resistivity and Temperature coefficient of resistivity (TCR) for alloys.

Alloy	ρ *10^{-8} (Ω.m)	TCR*10^{-3} (K^{-1})
Sn_{70}-Bi_{15}-Sb_{15}	239.0888	14.0558
Sn_{79}-Bi_{15}-Sb_{15}- In_1	200.2	5.9876
Sn_{67}-Bi_{15}-Sb_{15}- In_3	189.4736	4.7643
Sn_{65}-Bi_{15}-Sb_{15}- In_5	155	4.0307
Sn_{63}-Bi_{15}-Sb_{15}- In_7	126	3.8866
Sn_{61}-Bi_{15}-Sb_{15}- In_9	92.5	3.3571

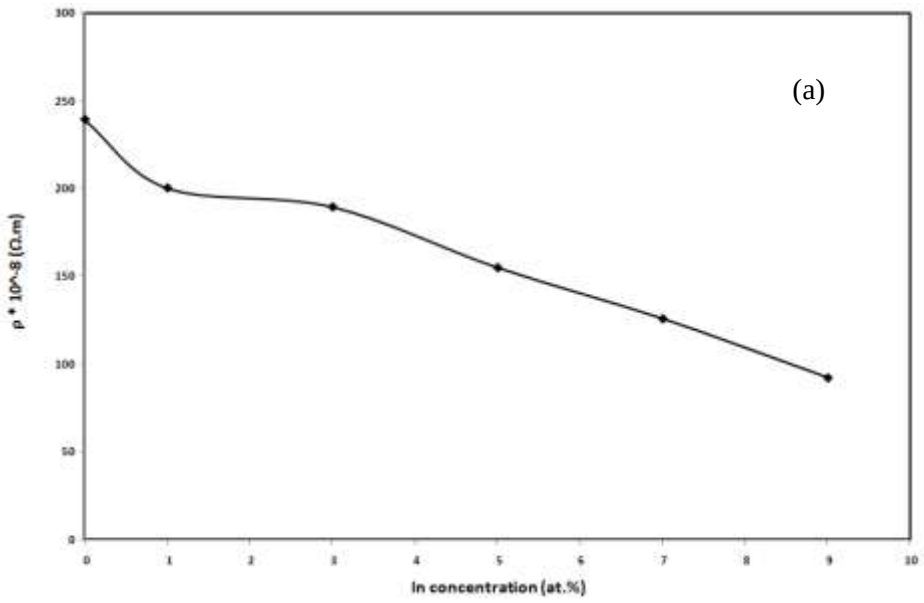

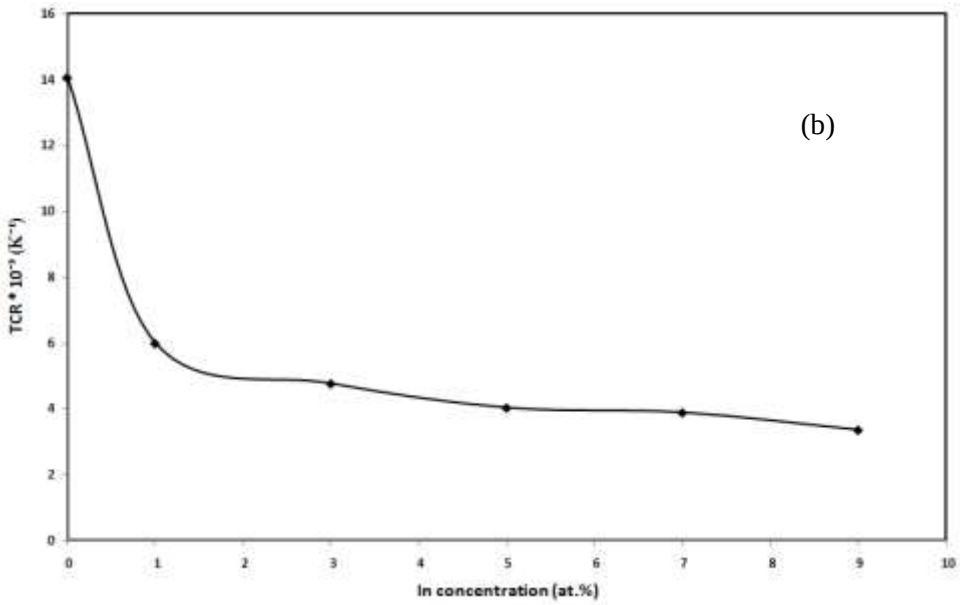

Figure 6. (a) the variation of ρ at room temperature with In concentration, (b) the variation of TCR with In concentration.

Table (V). conductivity, concentration of conduction electrons, mobility, and collision time and mean free path for all alloys.

Alloy	σ *10^{-5} (Ω.m)$^{-1}$	Concentration of conduction electrons (10^{23})	μ (m^2/V.S)	collision time (t) (s) (10^-17)	l (mean free path) (m) (10^-17)
Sn_{70}-Bi_{15}-Sb_{15}	4.1825	1.52008	17.1735	0.5880	0.1075
Sn_{79}-Bi_{15}-Sb_{15}- In_1	4.9950	1.51696	20.5517	0.7036	0.1807
Sn_{67}-Bi_{15}-Sb_{15}- In_3	5.2777	1.51073	21.8047	0.7465	0.1915
Sn_{65}-Bi_{15}-Sb_{15}- In_5	6.4516	1.50448	26.7650	0.9164	0.2347
Sn_{63}-Bi_{15}-Sb_{15}- In_7	7.9365	1.49823	33.0626	1.13204	0.2713
Sn_{61}-Bi_{15}-Sb_{15}- In_9	10.8108	1.49197	45.2255	1.54849	0.3940

2.4 Mechanical Properties

Elastic modulus (E), Shear modulus (G), Bulk modulus (B) and Poisson's ratio are calculated by dynamic resonance method for Sn_{70-x}-Sb_{15}-Bi_{15}-In_x alloys, x=0, 1, 3, 5, 7 and 9 at. %) [30,31]. It is investigated that (E) increases gradually with increasing the amount of In present which shown as in figure (7) up to 39.02708 GPa to Sn_{61}-Sb_{15}-Bi_{15}-In_9 alloy. It has been found that the additions of In in SnSbBiIn as melt-quenched ribbons improve the elastic moduli and it is attributed to the substantial refinement of the solidification microstructure. The mechanical results are shown in Table (VI). It is seen that there is a gradual increase in values of the mechanical properties with the amount of In content.

It was found that, the existence of metastable structural configurations at the interface and the internal strain distribution can obviously affect the mechanical behavior. This part reports some results of elasticity or internal friction measurements coupled to thermal diffusivity analysis on Sn_{70-x}-Sb_{15}-Bi_15-In_x melt-quenched ribbons using chill-block melt-spin technique [32-33].

ISSN 2347-3487
Volume 12 Number 2
Journal of Advances in Physics

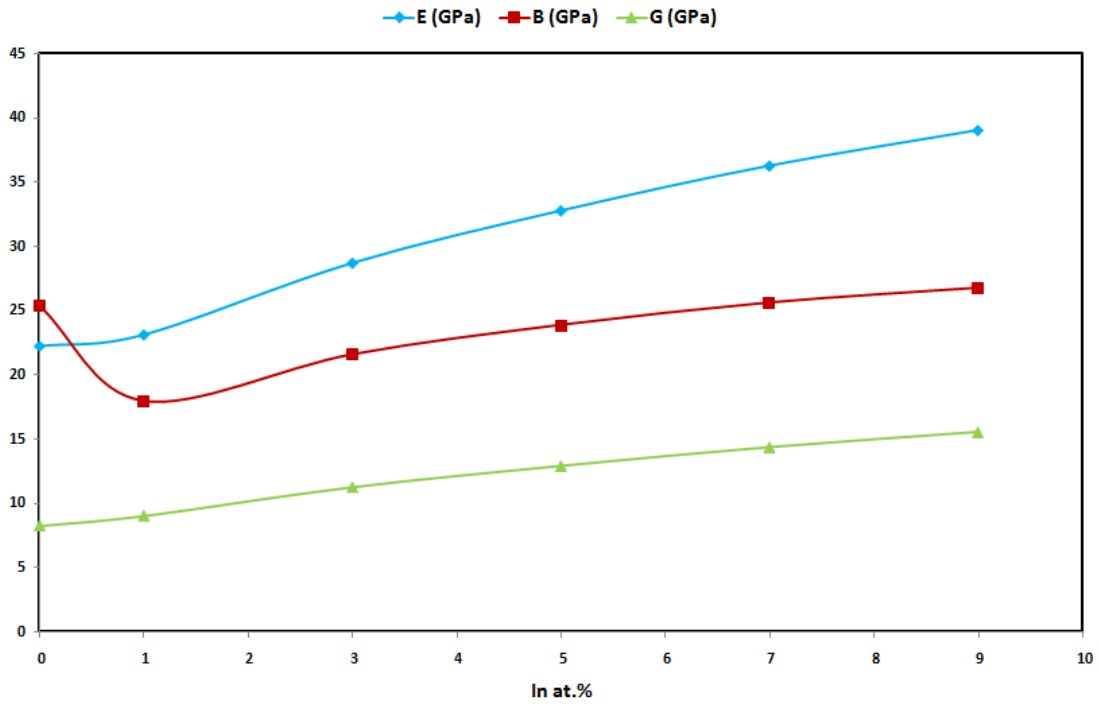

Figure (7). The Elastic modulus (E), Shear modulus (G), Bulk modulus and Poisson's ratio for Sn_{70-x}-Sb_{15}-Bi_15-In_x alloys.

Table (VI). The Elastic modulus (E), Shear modulus (G), Bulk modulus and Poisson's ratio for Sn_{70-x}-Sb_{15}-Bi_15-In_x alloys.

Alloy	E (GPa)	B (GPa)	G (GPa)	G/E	N
Sn_{70}-Bi_{15}-Sb_{15}	22.21295	25.35725	8.202716	0.369276	0.354
Sn_{79}-Bi_{15}-Sb_{15}- In_1	23.09387	17.9022	8.98590	0.389105	0.285
Sn_{67}-Bi_{15}-Sb_{15}- In_3	28.68701	21.53631	11.22344	0.391238	0.277
Sn_{65}-Bi_{15}-Sb_{15}- In_5	32.76205	23.83232	12.88946	0.393427	0.27
Sn_{63}-Bi_{15}-Sb_{15}- In_7	36.25926	25.58243	14.34561	0.39564	0.263
Sn_{61}-Bi_{15}-Sb_{15}- In_9	39.02708	26.73069	15.52804	0.397879	0.256

There are several equations to do these analyses. It is easy to show that the logarithmic decrement δ of the free vibration amplitude is simply related to the internal friction Q^{-1}. When the damping is small, the internal friction Q^{-1} is expressed by the formula:

$$Q^{-1} = \frac{\delta}{\pi} \qquad (3)$$

Where, δ is the logarithmic decrement and defined as the natural logarithm of the ratio of successive amplitudes. Then:

$$\delta = \frac{\ln\left(\frac{A_1}{A_2}\right)}{\left(\frac{t_1}{t_2}\right)f} \approx \frac{1}{2}\frac{\Delta E}{E} \qquad (4)$$

Where, A_1 and A_2 are the amplitudes at times t_1 and t_2, f is the natural frequency of the free – vibrating system, Δ E is the energy lost per cycle and E is the stored vibration energy.

The internal friction is very sensitive to the small changes in the mechanical state of the melt-spun ribbons and it can be used to measure thermal diffusivity. From the frequency f , at which the peak damping occurs, thermal diffusivity D_{th} is simply related to the frequency f by the formula :

$$D_{th} = \frac{2d^2 f}{\pi} \qquad (5)$$

Where d is the thickness of the ribbon .The measured values for internal friction Q^{-1} and thermal diffusivity D_{th} are listed in Table (VI). The data indicate that the internal friction is quite small and rapidly decrease friction in higher In content for Sn_{61}-Bi_{15}-Sb_{15}-In_9 in atomic percent for melt-quenched ribbons. Increasing indium concentrations the thermal diffusivity D_{th} is increasing.

Table (VII). Internal fraction (Q^{-1}) and thermal diffusivity (D_{th}) for Sn_{70-x}-Sb_{15}-Bi_15-In_x alloys.

Alloy	Q^{-1} (10^{-3})	D_{th} (m^2/s) * 10^{-8}
Sn_{70}-Bi_{15}-Sb_{15}	31.0742	1655.2114
Sn_{79}-Bi_{15}-Sb_{15}- In_1	26.9451	1765.1008
Sn_{67}-Bi_{15}-Sb_{15}- In_3	17.6514	1908.2901
Sn_{65}-Bi_{15}-Sb_{15}- In_5	13.1836	1993.5212
Sn_{63}-Bi_{15}-Sb_{15}- In_7	10.1961	2100.0789
Sn_{61}-Bi_{15}-Sb_{15}- In_9	6.6179	2535.4966

Thermal conductivity (K) may be calculated from the following equation:

$$K = 5.02\,\sigma\,T * 10^{-9} + 0.03 \qquad (6)$$

Where, T is the absolute temperature [34]. The mathematical formula that relates thermal diffusivity D_{th} to thermal conductivity K is given by:

$$D_{th} = \frac{K}{C_p \rho} \qquad (7)$$

Where, C_p is heat capacity and it is the temperature-dependent at constant pressure, and ρ is the density, as shown in Table (VIII). A typical values of thermal conductivity in units ($W.m^{-1}.k^{-1}$). The information is necessary for modeling the optimum conditions during processing.

Table (VIII). Electrical conductivity (σ), Thermal conductivity, density (ρ), and specific heat (C_p) for Sn_{70-x}-Sb_{15}-Bi_15-In_x alloys.

Alloy	σ *10^5 $(\Omega.m)^{-1}$	K *10^{-1} (W/m.K)	ρ (g / cm^3)	C_p (j/Kg.K)
Sn_{70}-Bi_{15}-Sb_{15}	4.1825	0.3763	5.7142	397.8828
Sn_{79}-Bi_{15}-Sb_{15}- In_1	4.9950	0.4494	7.9769	319.1966
Sn_{67}-Bi_{15}-Sb_{15}- In_3	5.2777	0.4748	6.4285	387.0992
Sn_{65}-Bi_{15}-Sb_{15}- In_5	6.4516	0.5804	5.9285	491.1650
Sn_{63}-Bi_{15}-Sb_{15}- In_7	7.9365	0.7141	5.5357	614.2571
Sn_{61}-Bi_{15}-Sb_{15}- In_9	10.8108	0.9727	4.5879	836.2000

3. Conclusion

From the present study the data shows that:

- From the analysis of X-ray diffraction result has proved that Sn_{70-x}-Sb_{15}-Bi_15-In_x , the alloy composed of tetragonal Sn , rhombohedral Bi phases, with a few lines form Sb phase, In phase, Bi_3In_5, and SnSb, InSb, $In_{0.2}Sn_{0.8}$ intermetallic compounds.
- It is found that by increasing Indium content, the electrical resistivity value of SnBiSbIn melt-spun alloys decreases linearly. The scattering centers of the electrons decrease which leads to an increase of orderly atomic arrangement. The result is a net increase in the electrical conductivity.
- The temperature coefficient of resistivity (TCR) decreases with increasing Indium content.
- Melting temperature decreases with increasing Indium content. Alloys have thermal stability because there is no phase change before melting peaks and there is a good pasty range in alloy.

- It has been found that the additions of In in SnBiSb as melt quenched ribbons improve the elastic moduli and it is attributed to the substantial refinement of the solidification microstructure.
- Internal friction decreases by increasing Indium content.
- Sn_{61}-Bi_{15}-Sb_{15}- In_9 has best physically prosperities, such as high values of electrical resistivity, elastic moduli and poisson's ratio, with lower melting point comparison with Sn-Pb eutectic which is indicated in table IX.

Table (IX). Comparison between Sn_{61}-Bi_{15}-Sb_{15}- In_9 and Sn-Pb eutectic alloy.

Alloy	ρ *10^{-8} (Ω.m)	E (GPa)	u	T_m (K)
Sn_{61}-Bi_{15}-Sb_{15}- In_9	239.08	39.02	0.256	432.6
Sn-37Pb	14.6	35	0.4	456

References

1- Lead-Free Solder project, final report, National center for manufacturing science, Michigan, 1997.

2- K. Suganuma and K. Kim, “Sn-Zn Low Temperature Solders,” Journal of Materials Science: Materials for Electronics, Vol. 18, No. 1-3, 2007, pp. 121-127.

3- K. N. Subramanian and J. G. Lee, “Physical Metallurgy in Lead-Free Electronic Solder Development,” JOM Journal of the Minerals, Metals and Materials Society, Vol. 55, No. 5, 2003, pp. 26-32.

4- J. Glazer, “Metallurgy of Low Temperature Pb-Free Sol- ders for Electronic Assembly,” International Materials Review, Vol. 40, No. 2, 1995, pp. 65-93.

5- L. Duan, D. Q. Yu, S. Q. Han, H. T. Ma and L. Wang, “Microstructural Evolution of Sn-9Zn-3Bi Solder/Cu Joint during Long-Term Aging at 170°C,” Journal of Al- loys and Compounds, Vol. 381, No. 1-2, 2004, pp. 202- 207.

6- C. W. Hwang and K. Suganuma, “Joint Reliability and High Temperature Stability of Sn-Ag-Bi Lead-Free Sol- der with Cu and Sn-Pb/Ni/Cu Substrates,” Materials Sci- ence and Engineering, Vol. 373, No. 1-2, 2004, pp. 187-194.

7- H. L. Lai and J. G. Duh, “Lead-Free Sn-Ag and Sn-Ag-Bi Solder Powders Prepared by Mechanical Alloying,” Jour- nal of Electronic Materials, Vol. 32, No. 4, 2003, pp. 215-220. doi:10.1007/s11664-003-0212-1

8- H. W. Miao and J. G. Duh, “Microstructural Evolution in Sn-Bi and Sn-Bi-Cu Solder Joints Under Thermal Ag- ing,” Materials Chemistry and Physics, Vol. 71, No. 3, 2001, pp. 255-271.

9- Xianfen Li, Fangqiu Zu, Lanjun Liu, Jigang Li, Jie Chen, Chengming Hu,"Effect of Sn on reversibility of liquid–liquid transition in Bi–Sb– Sn alloys", Journal of Alloys and Compounds 453 (2008) 508–512 .

10- Dragan Manasijevic´, Jan Vrest’al, Dusko Minic´, Ales Kroupa , Dragana Zivkovic´,Zivan Zivkovi´c," Phase equilibria and thermodynamics of the Bi–Sb–Sn ternary system",Journal of Alloys and Compounds 438 (2007) 150–157.

11- Y.S. Hor, R.J. Cava,"Thermoelectric properties of Sn-doped Bi– Sb", Journal of Alloys and Compounds 479 (2009) 368–371.

12- Alberto Torres, Luis Hernández, Octavio Domínguez,"Effect of Antimony Additions on Corrosion and Mechanical Properties of Sn- Bi Eutectic Lead-Free Solder Alloy",Materials Sciences and Applications, 2012, 3, 355-362 .

13- I.Ohnuma,X.J.Liu,H.Ohtani,K.Ishida,J.Electron.Mater.28(No.11)(1999) 1164-1171.

14- H.Ohtani and K.Ishida, J. Electron. Mater., (1994),23, 747- 755.

15- F.Ajersch and I.Ansara: Rapport L. T. P. C. M. TM01, E.N.S.E.E.G.,St.Martin d Heres,(1974).

16- A.B.Bhatia and N.H.Pelton:Can.Metall.Quart. 14(1975)213-219.

17- S.S.Balakrishna and A.K.Mallik: Sci.Forum 3(1985)405-417.

18- A.D.Pelton and C.W.Bale : Metall.Trans.17A(1986)1057-1063.

19- Y.Feutelais, G.Morgant, J.R.Didry and J.Schnitter :CALPHAD 16(1992)111-116 .

20- Mustafa Kamal, Abu-Baker El-Bediwi and Tarek El-Ashram, Journal of Materials science in Electronics 15(2004) 211-217.

21- Rizk Mustafa Shalaby and Mustafa Kamal, International Journal of physic and Research (IJPR), Vol.13,Issues,Dec.(2013),51-60.

22- Mustafa Kamal, Shalabia Badr and Nermin Ali Abdelhakim, International Journal of Engineering and Technology IJET-IJENS Vol: 14, No: 01 Feb.(2014) IJENS, PP:119-129.

23- Mustafa Kamal, Abu-Baker El-Bediwi and Jamal Khalil Majeed, International Journal of Engineering and Technology IJET-IJENS Vol.14, No: 02 April(2014) IJENS, PP: 5 -15 .

24- Mustafa Kamal and Usama S. Mohammad, A Review: Chill- Block Melt Spin Technique, Theories & Applications, Bentham e Books, Bentham science Publishers eISBN:978-1-60805-151- 9,(2012).

25- A.M. Shaban and M. Kamal, Radiation Effects and Defects in Solids, (1995),Vol.133, PP:5-13 .

26- B.D. Cullity," Elements of X-ray Diffraction", Addison–Wesley publishing company, INC, printed in the United States of American, (1959)PP: 263-265.

27- G.K. Williamson and W. H. Hall, Acta Metall. 1, 22-31(1953).

28- G. E. Doan, The Principles of Physical Metallurgy ,McGraw-Hill Book Company , Inc. 52-743 (1953) PP:215-217.

29- C.Zener,"Elasticity and Anelasticity of Metals",The University of Chicago press, Chicago , (1948).

30- E.Bonetti, L.Del Bianco , L.Pasquini, E.Sampaolesi, Nano Structured Materials, Vol.10,No.5,PP:741-753(1998).

31- J.J.Gilman, Journal of Applied Physics,Vol.46,No.4,April (1975)PP: 1625-1633.

32- J.M. Ide,"Some Dynamic Methods of Determination of Young's Modulus", Rev. Sci. Instr.,6: 296 (1935).

33- E. Schreiber, O. L. Anderson, and N. Soga,"Elastic Constants and their Measurements", McGraw-Hill Book Company (1973)PP:82-123.

34- Mustafa Kamal and Abu-Baker El-Bediwi, Journal of Materials science: Material in Electronics 11(2000)519- 523.

Author' biography with photo

1. Sara Mosaad Mahlab

Ph.D. Student.

Assistant lecturer in Physics department,

Faculty of Science,

Suez Canal University,

Egypt.

2. Prof. Dr. Abd El- Raouf M.

Prof. of solid state physics, physics department,

Faculty of Science, Port-Said University,

Egypt.

3. Prof. Dr. Mustafa Kamal M. Youssef

Prof. of Metal Physics, Physics department,

Faculty of Science, Mansoura University,

Egypt.